IET Computer Vision

Special Section: Selected Papers from the 19th International Conference on Image Analysis and Processing (ICIAP) 2017

IET Journals
The Institution of Engineering and Technology

Diffusion sensitivity enhancement filter for raw DWIs

ISSN 1751-9632
Received on 16th April 2018
Accepted on 18th July 2018
E-First on 10th September 2018
doi: 10.1049/iet-cvi.2018.5213
www.ietdl.org

Joshin John Mathew[1], Alex James[2] ✉, Chandrasekhar Kesavadas[3], Joseph Suresh Paul[4]

[1]*Computer Vision Team, ARS Traffic and Transport Technology, Trivandrum, India*
[2]*Department of Electrical and Computer Engineering, Nazarbayev University, Astana, Kazakhstan*
[3]*Department of Imaging Sciences and Interventional Radiology, SCTIMST, Trivandrum, India*
[4]*Medical Image Computing and Signal Processing Group, IIITM-K, Trivandrum, India*
✉ *E-mail: apj@ieee.org*

Abstract: In this study, a post-processing filter to enhance diffusion sensitivity, resulting in larger intensity changes in regions with the abrupt transition of local diffusivity in raw diffusion weighted image (DWI) volumes. Weights computed using a non-linear three-dimensional neighbourhood operation are assigned to each voxel within the neighbourhood, with the weighted average representative of the enhanced DWI. The processed images exhibit better distinction among regions with differing levels of physical diffusion. While the resulting improvements in diffusion sensitivity are highlighted with the help of colour maps, parametric maps, and tractography, implications of the filtering process to recover missing information is illustrated in terms of ability to restore portions of fibre tracts which are otherwise absent in the unprocessed diffusion tensor imaging. Quantitative evaluation of the filtering process is performed using a metric representative of the estimated *b*-value, which is the consolidation machine parameters used for DWI acquisition.

1 Introduction

Diffusion tensor imaging (DTI) is a magnetic resonance imaging technique for three-dimensional (3D) characterisation of spin diffusion leading to an analysis of white matter fibre orientation [1–8]. DTI is formulated based on the fact that directions of dominant spin diffusion are aligned along the orientation of fibre tracts [9–17]. Diffusion tensor (D) quantifies the diffusion at each voxel that is computed from a set of diffusion weighted image (DWI) volumes [18–20]. Parametric maps derived from D are then used for quantification and visualisation of fibre bundle orientations. In this paper, we address two main issues related to post-processing: (i) increase the reliability of missing tract estimation and (ii) localised filtering to enhance diffusivity changes.

It is well known that the reliability of fibre tract estimation depends on the sequence parameters used for acquisition. It also depends on the methods used for tract reconstruction and post-processing techniques employed to improve the accuracy of diffusion tensor calculation. In particular, the failure to visualise crossing, branching, and kissing fibres in addition to the depiction of the fibre termination point can result in suboptimal tractography. Further to add to the complexities in each processing step, different post-processing softwares for fibre tracking have known to yield reconstructions that are quite different. A popularly accepted form of clinical validation method consists of analysing the resulting fractional anisotropy (FA) maps acquired either as grey scale or colour images for interpretation of results by both quantitative and qualitative image analysis. More often, the FA maps fail to provide true depictions of fibres at locations of low signal amplitudes including those with crossings and acute angulations. This results in either the radiologist avoiding commenting or giving a wrong interpretation. Hence, it is essential to develop post-processing tools that can help visualise fibres that are not seen due to a poor signal to noise ratio, anisotropy, or angulation.

In connection with the second problem to be addressed, it is noteworthy that considering a three-factor dependence of the quality and usability of DTI derived visualisations. The first factor signifies a form of diffusion sensitivity that resolves differences between fast and slow diffusions at neighbouring voxels. This is typically a function of machine parameters involved in DWI acquisition and referred to as the b-value. The second factor consists of the number of DWI volumes acquired along different non-colinear gradient diffusion weighing directions (DWDs) [21–24]. Increase in number of DWD (nDWD) leads to improved accuracy of tensor computation [25, 26]. Finally, better image acquisition with reduced noise levels also contributes to the improved accuracy of tensor computation [27–33]. A key concern in support of the current processing requirements to address the second problem arises from the physical limitations in increasing the b-value [34, 35] and acquisition time with an increase in nDWD. Although methods exist for mitigation of noise effects [36–39], none of these has addressed the problem of improving image quality in terms of resolving fast and slow diffusions. The most widely used DTI post-processing techniques include various forms of anisotropic diffusion filters (ADF) [40–43], non-local means (NLM) filtering [44–49], wavelet-based noise reduction [50–52], and Weiner filtering [51, 53].

Since diffusion weighing is expressed in terms of an amount of signal attenuation, fast diffusion corresponds to low intensity regions. In the proposed method, the filtered intensities are such that lower intensities are further reduced, and higher intensities are further enhanced using a localised non-linear spatial filtering model. This is equivalent to computationally improve the diffusion sensitivity. The filtering step consists of choosing a fixed 3D neighbourhood region around each voxel. Weights are then assigned to each neighbourhood voxel based on the respective voxel intensity differences and the weighted average is replaced as the diffusion sensitivity enhanced voxel value. The sensitivity enhancement is mainly determined by the neighbourhood size. The filtering is presented in two forms: global and spatially adaptive approaches. In the former, the neighbourhood size is fixed for all voxels and chosen using a search procedure. The search consists of computing a measure signifying the *degree of sensitisation* for an increasing order of neighbourhood sizes. A size corresponding to the maximum degree of sensitisation is then chosen. In the adaptive approach, a search is performed for each voxel in an increasing order of neighbourhood sizes, where the neighbourhood size with maximum diffusion sensitivity enhancement (which is the difference between original and enhanced intensities) is chosen for the filtering operation. The procedure is then repeated for every other voxel. A summary of the procedure is shown in Fig. 1.

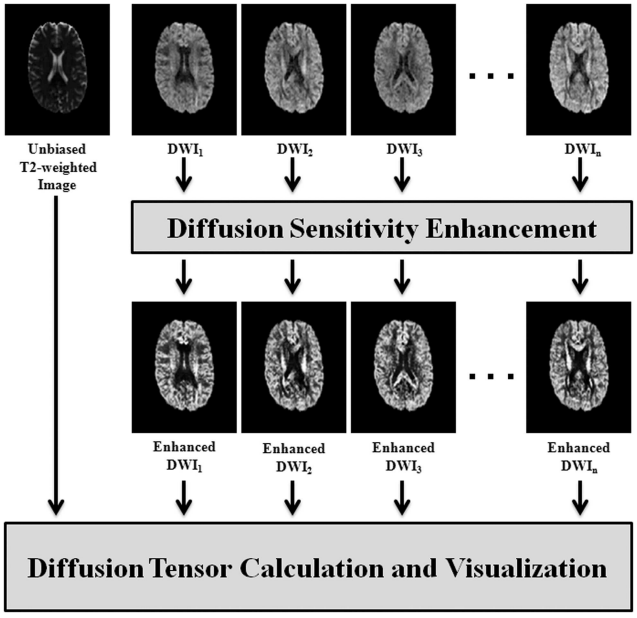

Fig. 1 *Pictorial representation of the proposed scheme*

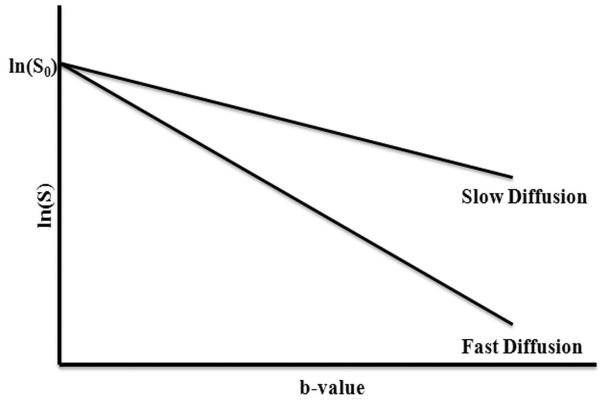

Fig. 2 *Diffusion sensitivity as a function of b-value*

As the proposed method is using diffusion weighted signals selected from a neighbourhood, it helps in a form of normalised enhancement throughout the image. This leads to better diffusion distinction to be achieved in both regions with high and low diffusion rates. Especially in regions with low diffusion rate, the neighbourhood will be representing voxels of similar diffusion rate and local operation contributes to maximising the numerical difference between them. As a result, local diffusion pattern dissimilarity will be increased, leading to better local anisotropy profile. This is the key factor in revealing an anisotropic profile with more stable diffusion directionality in respective tensors. This increase in diffusion directionality in regions suffering due to suboptimal tractography helps to increase the magnitude of measured anisotropy (better FA values). Increase in FA value thus shifts more suboptimal tractography regions to optimal tractography regions. This impact on tractography performance with the use of the proposed filter is shown by the restoration or visualisation of more white matter anatomy (tracts) in regions having low FA values before filtering.

2 Theory

2.1 Diffusion TI

Physical diffusion in brain tissues is measured using a Stejskal–Tanner imaging sequence [54] together with a gradient constituting a pair of dephase–rephase pulses. The amount of diffusion in each voxel is measured in terms of the signal attenuation with reference to a non-diffusion weighted baseline signal [55–60]. The signal equation of DWI is expressed as the equation below:

$$S = S_0 e^{-\gamma^2 G^2 \delta^2 (\Delta - (\delta/3))D} = S_0 e^{-bD} \tag{1}$$

S_0 is the magnetic resonance signal with no diffusion sensitisation, γ is the gyro magnetic, G denotes the magnitude of the applied gradients ($G = [g_x, g_y, g_z]$), δ is the pulse width of the individual gradient, Δ is the time interval between the centres of dephase and rephase pulses, and D is the diffusion coefficient. Higher b-value helps to achieve better diffusion sensitivity (Fig. 2).

DWI is capable of providing the net amount of physical diffusion for a given voxel location. In DTI, the diffusion coefficient is regarded as a tensor with values along all radial directions. When the diffusivity is considered to be vectors, the surface encompassing the tip of each vector is treated as an ellipsoid with principal axes orientated along directions represented by orthonormal unit vectors ν_1, ν_2, and ν_3. Denoting the lengths of each axis as λ_1, λ_2, and λ_3, the diffusion tensor D is given by the equation below:

$$\boldsymbol{D} = V \begin{bmatrix} \lambda_1 & 0 & 0 \\ 0 & \lambda_2 & 0 \\ 0 & 0 & \lambda_3 \end{bmatrix} V^{\mathrm{T}} \tag{2}$$

where $V = [\nu_1, \nu_2, \nu_3]$. From (2), D is now represented as a symmetric 3×3 matrix with elements consisting of the diffusion coefficients along xx, yy, zz, xy, yz, and xz directions. As there are six unknown diffusion coefficients, a minimum of six DWI volumes is used to compute D. The quality of DTI derived visualisations can be improved either by increasing the diffusion sensitivity or accurately estimating the diffusion tensor coefficients at each location. The maximisation of b-value is achieved by maximising the parameters such as γ, G, and Δ. The limitations in the maximisation of these three parameters [34, 35] are (i) increasing Δ reduces tissue contrast, (ii) δ is limited by Δ, and (iii) increasing G is limited by hardware constraints. Furthermore, increasing nDWD is constrained by increasing requirement of time and space for acquiring and storing a large number of DWI volumes. The approaches discussed above are restricted due to their physical limitations. Further quality improvement can only be possible by application of pre-filtering methods applied to raw DWI volumes.

2.2 Measured brain anisotropy and fibre tracking

Tractography algorithms relay on the measured anisotropy per-voxel and track the direction of physical diffusion by which identifying white matter fibre tract/bundles [61–67]. Tractography methods use diffusion tensors to compute dominant diffusion direction by means of eigendecomposition as described in the above section. This indicates toward the dependency between correctness and strength of measured anisotropic diffusion and fibre tracking algorithms.

FA map is a DTI derived quantification representing the relative amount of voxel-wise anisotropy. Ideally, FA assumes value 1 when the voxel is of maximum anisotropic nature and 0 for isotropic nature. Even though the white matter is anisotropic, due to the variations in tissue types and fibre bundle crossings the measured diffusion rate may vary from region to region. This variation can be clearly seen from varying intensities in FA maps [3] [for example, the cortex has low measured anisotropy (FA < 0.2)].

Fig. 3 shows a sample FA map (Fig. 3*a*) and fibre tracts computed (coloured regions in Fig. 3*b*) for the same slice. It is clearly visible that tracts are not computed at regions with low FA values. The plot represents the comparison between normalised histograms computed from FA values belonging to regions, where the tractography algorithm succeeds in finding fibre tracts and regions where it has failed. The plots depict a clear picture on the favourable and unfavourable FA range for fibre tracking algorithms. It is shown that the regions where tracking was not possible have FA values <0.2–0.3 range, whereas the tracking was possible beyond that range (that is FA > 0.2).

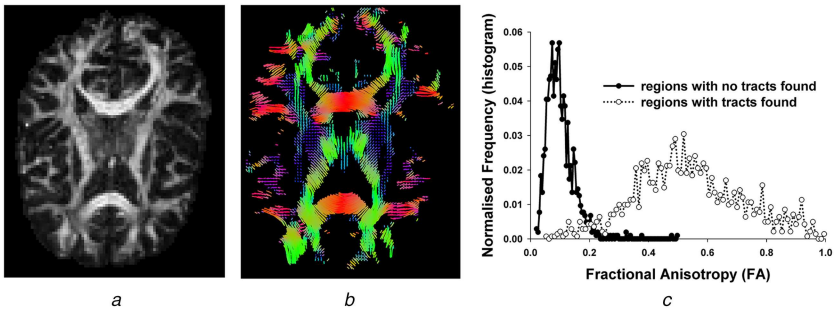

Fig. 3 *Comparison of favourable and unfavourable FA range for fibre tracking algorithms. From FA map*
(a) Fibre tracts computed, ***(b)*** It is visible that tracking fails in the region with low FA values and a normalised histogram of FA values, ***(c)*** Regions with tracts have a favourable FA range >0.2. The resolution of the images is of 128 × 128

1: **function** $SEF(S, w)$ ▷ Where S: DWI volume, w: neighborhood or kernel size
2: IND = all the indices or voxel locations in S
3: $K_{size} = w^3$
4: **for** $i = 1$ to $length(IND)$ **do**
5: w_{kernel} = $3D$ neighborhood or kernel of size w, selected at i^{th} location of S
6: $S_e = 0$
7: **for** $j = 1$ to K_{size} **do**
8: $diff = S(i) - w_{kernel}(j)$
9: $kernel = W(diff)$, W is weight calculation function
10: $S_e = S_e + \frac{w_{kernel}(j) \times kernel}{K_{size}}$
11: $S_f(i) = S(i) + S_e$
12: S_f is the diffusion sensitivity enhanced DWI volume

Fig. 4 *Algorithm 1: Sensitivity enhancement filter (SEF)*

It can be concluded that FA values beyond a threshold become necessary for robust fibre tracking. This is the motivation for this paper and a post-processing of raw DWI data is proposed to improve local distinction between measured physical diffusions (in DWI, it is in the form of signal attenuation). A clear distinction between nearby differing diffusion levels is thus improved, leading to betterment in measure anisotropy values. As the proposed method focuses on the enhancement of diffusion distinction or in other words a computational approach to achieve diffusion sensitivity enhancement, the method is referred to as *diffusion sensitivity enhancement filtering*.

3 Proposed method

Increased diffusion sensitivity improves the numerical distinction between diffusion weighing in DWI depending on the region-wise varying physical diffusion levels. The numerical difference between region-wise diffusion weighted signals determines the strength of measured anisotropy. Hence, the approach is to maximise the existing numerical difference between neighbouring regions based on the intensities distribution selected from a given neighbourhood size. Neighbourhood operation results in the enhancement of local anisotropic patterns and helps in the better measurement of anisotropy in both high and low diffusion regions. Thus, the required enhancement filter should be capable of maximising the numerical distance between regions based on local diffusion profile.

The proposed filtering method defines the enhanced DWI (S_f) expressed as the summation of original intensity (S) and the weighted average of neighbouring voxels (S_e), (3) [Algorithm 1 (see Fig. 4) step 11]

$$S_f = S + S_e \tag{3}$$

where S_e is computed using a non-linear filter applied to the original DWI S. For a cubic neighbourhood ($w \times w \times w$) with R pixels, S_e is expressed as below [Algorithm 1 (Fig. 4) steps 5–10]:

$$S_e(p) = \frac{1}{R}\sum_{i=1}^{R} k(i)S(p)(i) \tag{4}$$

where $k(i)$ represents the weight calculated at the ith kernel location, p is the reference voxel location on raw DWI data, and S (1) which is enhanced using the proposed filtering. $k(i)$ is considered as a function of positive and negative grey-level differences $[\delta S(i) = S(p) - S(i)]$. S_e has a very important role in determining the degree to which S is enhanced. It is because S_e eventually signifies or quantifies the difference between different diffusion levels in the enhanced versions of S. Thus, maximising S_e leads to an increased resolution between neighbouring regions. For deriving the weights for each neighbourhood voxel, the S_e can either be an addition or subtraction. The extremum cases are separately shown in the equations below:

$$S_f(p) = S(p) + \frac{1}{R}\sum_{i=1}^{R} S(p) \tag{5}$$

with $k(i) = 1, \ \forall i$ and

$$S_f(p) = S(p) - \frac{1}{R}\sum_{i=1}^{R} S(p) \tag{6}$$

with $k(i) = -1, \forall i$. Also, the minimum or zero degrees of enhancement will result when S_e assumes a value equal to 0. Using (5) and (6), the weight calculation function $W[\delta S(i)]$ can be summarised as below:

$$W(\delta S(i)) = \begin{cases} 1 & \text{if } \delta S(i) > 0 \\ 0 & \text{if } \delta S(i) = 0 \\ -1 & \text{if } \delta S(i) < 0 \end{cases} \tag{7}$$

Algorithm 1 (Fig. 4) outlines a pseudocode for the proposed method.

Neighbourhood sizes are determined from the spread of intensity uniformity at each location. Since the neighbourhood sizes can be locally determined, a mere global maximisation of the degree of sensitisation will not be sufficient to retrieve complete information on fibre orientations. Also, the practical applicability of the proposed method in real-time operations is limited by the time and space complexity involved in this approach.

In consideration of the above facts, the proposed method is modified to locally adapt the neighbourhood sizes at each location. In this approach, the filtering procedure is initiated with a small neighbourhood size at all locations [Algorithm 2 (see Fig. 5) step 3]. The values of $\| S_e \|$ at each location are then compared with those obtained using the next incremental step increase in neighbourhood size [Algorithm 2 (Fig. 5) step 10]. For every step change, locations that exhibit reduced values of $\| S_e \|$ are assigned the neighbourhood size corresponding to the previous step [Algorithm 2 (Fig. 5) step 11]. As the iteration proceeds toward larger neighbourhood sizes, the number of locations requiring

1: **function** $iSEF(S, w_0)$ ▷ Where S: DWI volume, w_0: initial neighborhood or kernel size
2: IND = all the indices or voxel locations in S
3: $w = w_0$ ▷ initialize kernel size w as w_0
4: **while** $sizeof(IND) > 0$ **do** ▷ runs till all pixel indices undergo filtering
5: $IND_1 = IND$ ▷ First index from IND
6: $IND = RemoveIndex(IND, 1)$ ▷ Removes first index value from IND
7: $\mu_0 = 0$ ▷ a variable to later store magnitude of S_e computed for the smallest kernel size from two consecutive kernel sizes w.r.t each iteration in optimum kernel size selection, initialized as 0
8: **while** $infinite$ **do** ▷ Infinite While loop
9: $\mu_{S_e} = ||S_{e,w}||$ ▷ magnitude of S_e w.r.t kernel size w computed at IND_1 voxel
10: **if** $\mu_0 > \mu_{S_{e,w}}$ **then** ▷ checks whether the magnitude of S_e for previous kernel size is greater than the immediate higher kernel size
11: $S_f(IND_1) = S(IND_1) + S_{e,w-2}$ ▷ diffusion sensitivity enhanced DWI value at IND_1 voxel, where S_e from previous kernel size $(w-2)$, $S_{e,w-2}$ is added to S
12: $\mu_0 = 0$ ▷ reset μ_0 as 0 for next index from IND
13: $w = w_0$ ▷ reset w as w_0 for next index from IND
14: **break** ▷ breaks while loop w.r.t IND_1 and proceeds to next index in IND
15: **else**
16: $\mu_0 = \mu_{S_{e,w}}$ ▷ update μ_0 as $\mu_{S_{e,w}}$ for comparison against next kernel size in next iteration
17: $w = w + 2$ ▷ w incremented to next size

Fig. 5 *Algorithm 2: Iterative window optimised model, iSEF*

further neighbourhood optimisation will decrease. This iterative approach significantly reduces the time and space requirements needed for the best possible filter performance. Algorithm 2 (Fig. 5) describes the key steps in the locally adaptive iterative filter.

4 Results

4.1 Neighbourhood size selection

Neighbourhood size selection is based on the maximisation of diffusion sensitivity. From (3) to (6), the diffusion sensitivity will be maximum when the magnitude of S_e assumes maximum value. The plot in Fig. 6 illustrates the choice of optimum neighbourhood size based on maximising the degree of sensitisation using the equation below:

$$S_{\text{degree}} = \max_{w} \left(\sum_{x,\,y} \| S_e(x,\,y) \| \right) \tag{8}$$

The improvement in region-wise distinction (RWD) of diffusion sensitised intensities is quantitatively illustrated in Table 1 with the help of a second measure, further referred to as *sensitisation difference measure (S_{DM})*. For a given region-of-interest (ROI), this is defined using the maximum and minimum intensities as formulated using the equation below:

$$S_{\text{DM}} = \frac{\max\,(S_{\text{ROI}}) - \min\,(S_{\text{ROI}})}{\max\,(S_{\text{ROI}}) + \min\,(S_{\text{ROI}})} \tag{9}$$

S_{DM} assumes values ranging from 0 to 1, with the 0 representing zero improvements in RWD, and 1 indicating maximum RWD for a given ROI. Table 1 shows S_{DM} values computed for arbitrarily chosen ROIs. The mean S_{DM} increases from 0.3823 for original (S) to 0.8108 for the filtered version (S_e).

Optimisation using a degree of sensitisation is meaningful only when S_e is computed using the same neighbourhood size at all locations. For the iterative window optimised model, it is found that the optimal window size for each location is different. Fig. 7

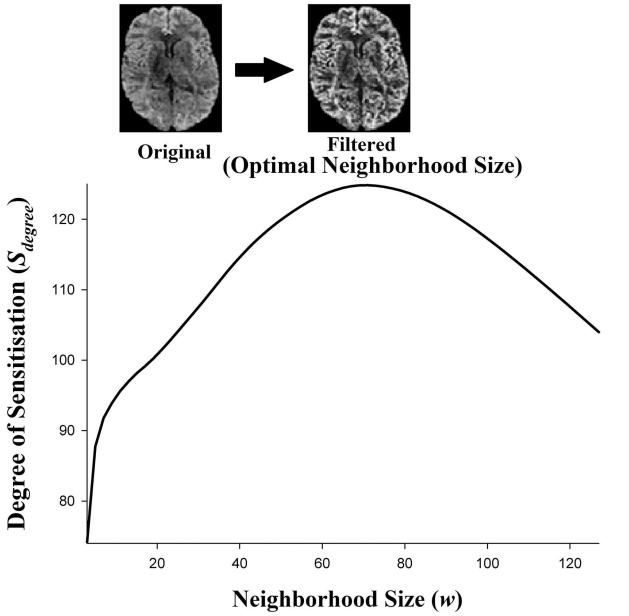

Fig. 6 *Optimum window size search; optimal neighbourhood/kernel size is chosen to correspond to maximum degree of sensitisation (*71×71*)*

shows the number of voxel locations optimised for each incremental neighbourhood size. It is observed that majority of voxel locations is optimised at the lower neighbourhood sizes. The number of voxel locations optimised at larger increments of the neighbourhood size decreases monotonically, thereby decreasing the spatial and time complexities.

Figs. 8*a*2–*d*2 display the optimal window sizes mapped to each voxel. Brighter regions correspond to larger neighbourhood sizes and vice versa. It is observed that regions representing a higher degree of diffusion require larger neighbourhood sizes for enhancement.

4.2 Qualitative analysis

Quality enhancement of DTI derivations achieved using other known approaches such as ADF, NLM filter, wavelet filter, and Weiner filter are compared against the proposed method. Qualitative analysis is performed with the help of FA maps, colour-coded orientation diffusion directions, and fibre tracts are computed using ExploreDTI. FA maps are the commonly used parametric maps for the quantification of anisotropy, where brightest region represents maximum anisotropy and vice versa. Colour-coded orientation maps provide information regarding the direction of the diffusion process. Such colour-coded orientation maps are further used in computing/tracking various fibre tracts for understanding brain connectivity between various brain faculties. Although gold standards are not available for quantifying the quality of DTI derivations, a relative evaluation is performed in terms of the robustness in computing fibre tracts in addition to visual comparison.

FA maps and colour-coded orientation maps are computed for two raw DTI data sets. The first data set (Dataset 1 obtained from ExploreDTI sample data) consists of 60 DWI volumes along with six non-diffusion weighted baseline volumes and the *b*-value used in image acquisition is 1210. The second data set (Dataset 2 obtained from University College London (UCL) camino) contains three unbiased T2-weighted volumes and 30 DWI volumes with a *b*-value of 1000.

Fig. 9 illustrates the colour-coded orientation maps and FA maps computed from original raw DTI and its various pre-processed versions for both datasets. From the visual evaluation of the results, it is seen that the proposed filter significantly enhanced the quality of signal strength and discrimination of fibre bundles in comparison with other filtering methods. On a closer observation, it is observed that the proposed filter is able to restore many fibre bundles which are hidden, and otherwise generates discontinuities in the unfiltered and other processed versions. The use of our

Table 1 Sensitisation difference measure computed for random ROIs

ROI	Sensitisation difference measure (S_{DM})	
	Original version (S)	Processed version (S_e)
1	0.5872	0.9625
2	0.4569	0.9900
3	0.5341	0.9966
4	0.4632	0.7804
5	0.2769	0.6706
6	0.1737	0.7371
7	0.3656	0.7864
8	0.3420	0.5954
9	0.2356	0.9377
10	0.3872	0.6510
average	0.3823	0.8108

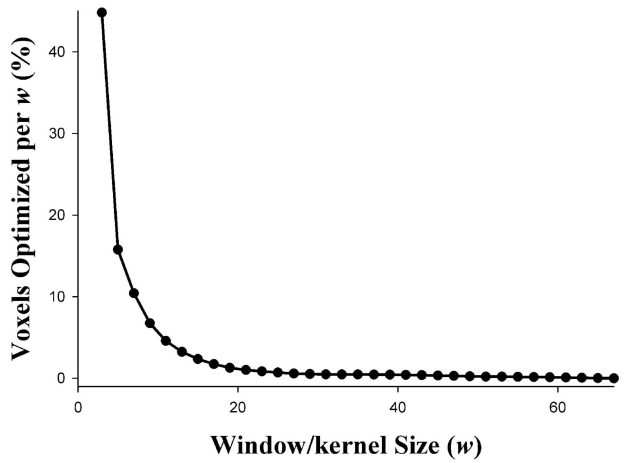

Fig. 7 *Number of voxel locations (in percentage) optimised for each window size, w for evaluating the iterative window optimised approach. There is a significant reduction in the number of voxel locations yet to be optimised for higher window size in subsequent iterations*

filtering also contributes to a better understanding of the boundaries between different bundles. This can be easily inferred from ventricular regions in both FA and colour maps. Better distinction between bundles will serve to improve the fibre tracking performance. Improved results for tractography are discussed in a later section. There is a tremendous and visible increase in the signal strength, leading to a better understanding of anisotropy inside the brain.

4.3 Fibre tracking

Robustness of tracking algorithms [61–67] in improving the distinction between computed tracts and the number of tracts identified for a given dataset is very important in brain connectivity studies. For these reasons, this paper compares the 2D fibre tracts computed for Dataset 1 (Fig. 10).

From Fig. 10, it is clearly seen that the proposed filter significantly improves the robustness of the tracking algorithm. As compared to the unfiltered data and other filtering methods discussed earlier, there is a clear increase in the number of tracts identified. The results also evidence restoration capabilities of the proposed filter. Furthermore, this increased number of computed tracts clearly shows that the proposed filter definitely improves the diffusion sensitivity.

5 Discussion and conclusion

DTI computes various parametric maps and colour-coded orientation diffusion direction maps from the 3×3 tensors, for visualisation and quantification of the physical diffusion characteristics [68–73]. Such DTI derivations are further used for

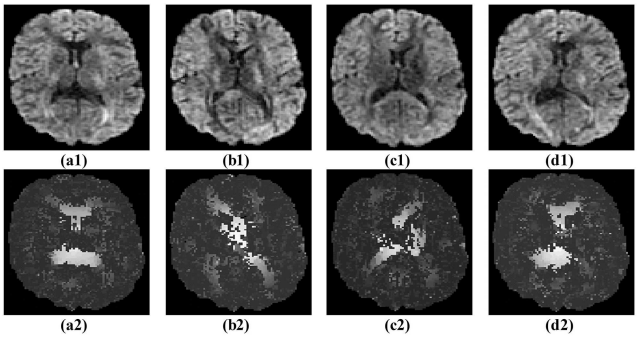

Fig. 8 *Optimal window size mapped at each voxel location*
(a1–d1) Input DWI slices, ***(a2–d2)*** Window size maps. Brighter regions display larger window sizes

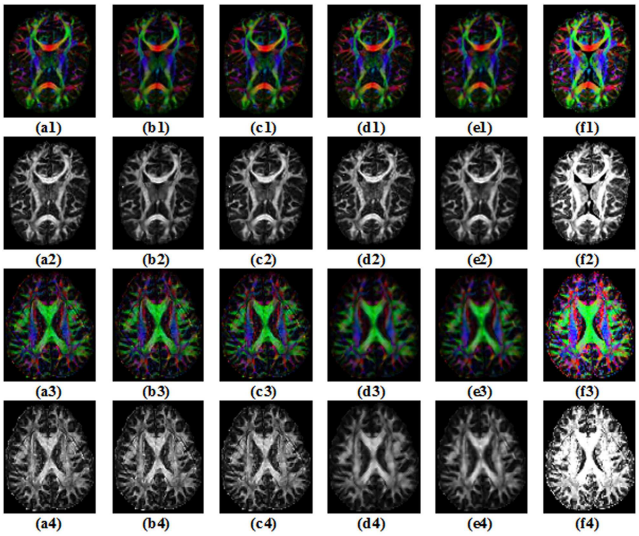

Fig. 9 *Colour-coded orientation maps (a1–f1, a3–f3) and FA maps (a2–f2, a4–f4) for Dataset 1 and Dataset 2*
(a1–a4) Unfiltered, ***(b1–b4)*** Anisotropic diffusion filtered, ***(c1–c4)*** NLM filtered, ***(d1–d4)*** Wavelet filtered, ***(e1–e4)*** Weiner filtered, and ***(f1–f4)*** current method

evaluating the quality of the diffusion sensitisation achieved by our filter.

Our filtering method improves the distinction between neighbourhood regions with different diffusion levels leading to sensitivity enhancement. The filter uses a 3D filtering operation to compute a non-linear weighted average (S_e) from the voxel neighbourhood and added to the original image (S) to obtain its enhanced version (S_f). The neighbourhood sizes are optimised using indirect measures that reflect the degree of sensitisation. The sensitivity enhancement is quantified and presented in Table 2 using three measures: (i) average increase in diffusion sensitivity (IDS), (ii) standard deviation of local diffusion sensitivity (σ_{DS}), and (iii) estimated b-value enhancement. The average IDS defined using mean($\| (S_f - S)/S_0 \|$) provides an indication of an increase in the magnitude of diffusion sensitisation. The standard deviation of local diffusion sensitivity defined using std(S_f/S_0) reflects a direct relationship to sensitivity. To understand the third measure, we first follow the signal equations for both filtered and unfiltered data. Denoting the original b-value and the enhanced b-value as b_0 and b_e and treating D to be an unchanged physical parameter independent of any post-processing step, the signal equations are expressed as the equations below:

$$S = S_0 e^{-b_0 D} \tag{10}$$

$$S_f = S_0 e^{-b_e D} \tag{11}$$

From the above equations (10) and (11), the enhanced b-value for each voxel is estimated as the equation below:

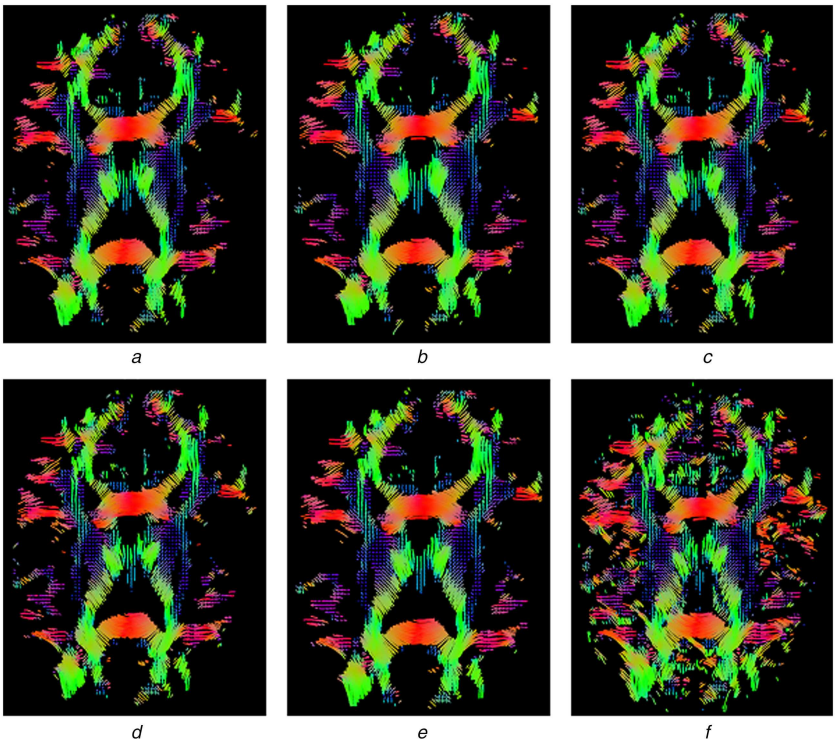

Fig. 10 *Tractography results*

(a) Fibre tracts computed (2D) for dataset 1, ***(b)*** Anisotropic diffusion filtered, ***(c)*** NLM filtered, ***(d)*** Wavelet filtered, ***(e)*** Weiner filtered, and ***(f)*** current method. Application of the proposed method helps in enhancing the efficiency and robustness of the fibre tracking algorithm. More tracts are identified with the improved distinction between fibre bundles, leading to a better understanding of the brain connectivity

Table 2 Comparison with other state-of-the-art methods

Data used	Average IDS	Standard deviation of local diffusion sensitivity (σ_{DS})	Estimated *b*-value from processed DWI versions (b_e)
original	not applicable	0.1423	1210
ADF [40–43]	0.0199	0.1300	1236
NLM [44–49]	0.0196	0.1379	1213
wavelet [50–52]	0.0248	0.1423	1210
Weiner [51, 53]	0.0278	0.1320	1236
globally optimised proposed	**0.1060**	**0.2244**	**1577**
iteratively optimised proposed	**0.1873**	**0.3005**	**1891**

Bold values show improved performance.

$$b_e = b_0 \frac{\log(S_f/S_0)}{\log(S/S_0)} \tag{12}$$

From Table 2, it is seen that other existing methods do not significantly contribute toward diffusion enhancement. In contrast, both global and iterative versions of our method exhibited notable improvement in diffusion sensitisation. In comparison to other state-of-the-art methods, application of our filter resulted in a five-fold increase in IDS using global version and nine-fold increase using iterative version. Along similar lines, the σ_{DS}, and the values were 1.5–2 and 1.3–1.6 times more compared with other state-of-the-art methods. Other methods used for comparison include ADF [40–43], NLM filter [44–49], wavelet-based noise reduction [50–52], and Weiner filter [51, 53].

In summary, the proposed method is found to be superior in terms of improving the distinction between fibre bundles. The method has illustrated its potential for restoration of regions (fibre tracts) which were otherwise not notable in the unprocessed versions. The results for FA maps, colour-coded orientation diffusion directions, and tractography show clear evidence for the above facts.

6 References

[1] Le Bihan, D., Jean-François, M., Poupon, C., *et al.*: 'Diffusion tensor imaging: concepts and applications', *Magn. Reson. Imaging*, 2001, **13**, pp. 534–546

[2] Basser, P.J., Jones, D.K.: 'Diffusion-tensor MRI: theory, experimental design and data analysis – a technical review', *NMR Biomed.*, 2002, **15**, pp. 456–467

[3] Mori, S., Zhang, J.: 'Principles of diffusion tensor imaging and its applications to basic neuroscience research', *Neuron*, 2006, **51**, pp. 527–539

[4] Jones, D.K., Leemans, A.: 'Diffusion tensor imaging', *Magn. Reson. Neuroimaging*, 2011, **711**, pp. 127–144

[5] Ryan, P.C., Bastinb David, E., Laidlawa, H.: 'A comparative evaluation of voxel-based spatial mapping in diffusion tensor imaging', *Neuroimage*, 2017, **146**, pp. 100–112

[6] Breton, M.A., DeKosky, S.T., James, R.C., *et al.*: 'Diffusion tensor imaging (DTI) findings in adult civilian, military, and sport-related mild traumatic brain injury (*m*TBI): a systematic critical review', *Brain Imaging Behav.*, 2018, **12**, pp. 585–612

[7] Mohammed, K., Emanuele, S., Ben, A.H.: 'A multicomponent approach to nonrigid registration of diffusion tensor images', *Appl. Intell.*, 2017, **46**, pp. 241–253

[8] Xianhua, Z., Shanshan, H., Weisheng, L.: 'Color perception of diffusion tensor images using hierarchical manifold learning', *Pattern Recognit.*, 2017, **63**, pp. 583–592

[9] Lazar, M., Weinstein, D.M., Tsuruda, J.S., *et al.*: 'White matter tractography using diffusion tensor deflection', *Hum. Brain Mapp.*, 2003, **18**, pp. 306–321

[10] Mattiello, J., Basser, P.J., Le Bihan, D.: 'Analytical expressions for the *b* matrix in NMR diffusion imaging and spectroscopy', *J. Magn. Reson.*, 1994, **108**, pp. 131–141

[11] Basser, P.J., Pierpaoli, C.: 'Microstructural and physiological features of tissues elucidated by quantitative-diffusion-tensor MRI', *J. Magn. Reson.*, 1996, **111**, pp. 209–219

[12] Pierpaoli, C., Jezzard, P., Basser, P.J., *et al.*: 'Diffusion tensor MR imaging of the human brain', *Radiology*, 1996, **201**, pp. 637–648

[13] Matteo, B., Michiel, C., Krikor, D., *et al.*: 'Improved tractography using asymmetric fibre orientation distributions', *Neuroimage*, 2017, **158**, pp. 205–218

[14] Walid, I.E., Fan, Z., Prashin, U., *et al.*: 'White matter tractography for neurosurgical planning: a topography-based review of the current state of the art', *Neuroimage Clin.*, 2017, **15**, pp. 659–672

[15] Miguel, G., Claudio, R., Josselin, H., *et al.*: 'Reproducibility of superficial white matter tracts using diffusion-weighted imaging tractography', *Neuroimage*, 2017, **147**, pp. 703–725

[16] Po-Shan, W., Chien-Li, Y., Chia-Feng, L., *et al.*: 'The involvement of supratentorial white matter in multiple system atrophy: a diffusion tensor imaging tractography study', *Acta Neurol. Belg.*, 2017, **117**, pp. 213–220

[17] Evangelia, T., Randall, E., Nader, P.: 'Using probabilistic tractography to target the subcallosal cingulate cortex in patients with treatment resistant depression', *Psychiatry Res., Neuroimaging*, 2017, **261**, pp. 72–74

[18] Mattiello, J., Basser, P.J., Le Bihan, D.: 'The *b* matrix in diffusion tensor echo-planar imaging', *Magn. Reson. Med.*, 1997, **37**, pp. 292–300

[19] Basser, P.J., Pierpaoli, C.: 'A simplified method to measure the diffusion tensor from seven MR images', *Magn. Reson. Med.*, 1998, **39**, pp. 928–934

[20] Papadakis, N.G., Xing, D., Huang, C.L., *et al.*: 'A comparative study of acquisition schemes for diffusion tensor imaging using MRI', *J. Magn. Reson.*, 1999, **137**, pp. 67–82

[21] Ming-Chung, C., Fong, K.E., Mori, S.: 'Effects of *b*-value and echo time on magnetic resonance diffusion tensor imaging-derived parameters at 1.5 T: a voxel-wise study', *J. Med. Biol. Eng.*, 2013, **33**, pp. 45–50

[22] Kim, H.J., Choi, C.G., Lee, D.H., *et al.*: 'High-*b*-value diffusion-weighted MR imaging of hyperacute ischemic stroke at 1.5 T', *Am. J. Neuroradiol.*, 2005, **26**, pp. 208–215

[23] Assaf, Y., Ben-Bashat, D., Chapman, J., *et al.*: 'High *b*-value *q*-space analyzed diffusion-weighted MRI: application to multiple sclerosis', *Magn. Reson. Med.*, 2002, **47**, pp. 115–126

[24] Jones, D.K.: 'The effect of gradient sampling schemes on measures derived from diffusion tensor MRI: an Monte Carlo study', *Magn. Reson. Med.*, 2004, **51**, pp. 807–815

[25] Zhang, N., Zhen-Sheng, D., Fang, W., *et al.*: 'The effect of different number of diffusion gradients on SNR of diffusion tensor-derived measurement maps', *J. Biomed. Sci. Eng.*, 2009, **2**, pp. 96–101

[26] Ni, H., Kavcic, V., Zhu, T., *et al.*: 'Effects of number of diffusion gradients on derived diffusion tensor imaging indices in human brain', *Am. J. Neuroradiol.*, 2006, **27**, pp. 1776–1781

[27] Gudbjartsson, H., Patz, S.: 'The Rician distribution of noisy MRI data', *Magn. Reson. Med.*, 1995, **34**, pp. 910–914

[28] Bastin, M.E., Armitage, P.A., Marshall, I.: 'A theoretical study of the effect of experimental noise on the measurement of anisotropy in diffusion imaging', *Magn. Reson. Med.*, 1998, **16**, pp. 773–785

[29] Basser, P.J., Pajevic, S.: 'Statistical artifacts in diffusion tensor MRI caused by background noise', *Magn. Reson. Med.*, 2000, **44**, pp. 41–50

[30] Skare, S., Li, T., Nordell, B., *et al.*: 'Noise considerations in the determination of diffusion tensor anisotropy', *Magn. Reson. Med.*, 2000, **18**, pp. 659–669

[31] Dietrich, O., Heiland, S., Sartor, K.: 'Noise correction for the exact determination of apparent diffusion coefficients at low SNR', *Magn. Reson. Med.*, 2001, **45**, pp. 448–453

[32] Anderson, A.W.: 'Theoretical analysis of the effects of noise on diffusion tensor imaging', *Magn. Reson. Med.*, 2001, **46**, pp. 1174–1188

[33] Jones, D.K., Basser, P.J.: 'Squashing peanuts and smashing pumpkins: how noise distorts diffusion-weighted MR data', *Magn. Reson. Med.*, 2004, **52**, pp. 979–993

[34] Mori, S.: '*Introduction to diffusion tensor imaging*' (Elsevier, Amsterdam, 2007)

[35] Akram, A., Michael, U.: '*Wavelets in medicine and biology*' (Elsevier, Amsterdam, 2007)

[36] Parker, G.M.J., Schnabel, J.A., Symms, M.R., *et al.*: 'Nonlinear smoothing for reduction of systematic and random errors in diffusion tensor imaging', *Magn. Reson. Med.*, 2000, **11**, pp. 702–710

[37] McGraw, T., Vemuri, B.C., Chen, Y., *et al.*: 'DT-MRI denoising and neuronal fiber tracking', *Magn. Reson. Med.*, 2004, **8**, pp. 95–111

[38] Chen, B., Hsu, E.: 'Noise removal in magnetic resonance diffusion tensor imaging', *Magn. Reson. Med.*, 2005, **54**, pp. 393–407

[39] McGraw, T., Vemuri, B., Ozarslan, E., *et al.*: 'Variational denoising of diffusion weighted MRI', *Inverse Probl. Imaging*, 2009, **3**, pp. 625–648

[40] Perona, P., Malik, J.: 'Scale-space and edge detection using anisotropic diffusion', *IEEE Trans. Pattern Anal. Mach. Intell.*, 1990, **12**, pp. 629–639

[41] Ding, Z., Gore, J.C., Anderson, A.W.: 'Reduction of noise in diffusion tensor images using anisotropic smoothing', *Magn. Reson. Med.*, 2005, **53**, pp. 485–490

[42] Xu, Q., Anderson, A., Gore, J., *et al.*: 'Efficient anisotropic filtering of diffusion tensor images', *Magn. Reson. Imaging*, 2010, **28**, pp. 200–211

[43] Deepak, M., Santanu, C., Mukul, S., *et al.*: 'Edge probability and pixel relativity-based speckle reducing anisotropic diffusion', *IEEE Trans. Image Process.*, 2018, **27**, pp. 649–664

[44] Buades, A., Coll, B., Morel, J.M.: 'A non-local algorithm for image denoising'. Proc. IEEE Int. Conf. Computer Vision and Pattern Recognition, 2005, vol. **2**, pp. 60–65

[45] Wiest-Daesslé, N., Prima, S., Coupé, P., *et al.*: 'Nonlocal means variants for denoising of diffusion-weighted and diffusion tensor MRI', *Proc. MICCAI*, 2007, **10**, pp. 344–351

[46] Coupé, P., Yger, P., Prima, S., *et al.*: 'An optimized blockwise nonlocal means denoising filter for 3D magnetic resonance images', *IEEE Trans. Med. Imaging*, 2008, **27**, pp. 425–441

[47] Descoteaux, M., Wiest-Daesslé, N., Prima, S., *et al.*: 'Impact of Rician adapted non-local means filtering on HARDI', *Proc. MICCAI*, 2008, **11**, pp. 122–130

[48] Manjón, J.V., Coupé, P., Martí-Bonmatí, L., *et al.*: 'Adaptive non-local means denoising of MR images with spatially varying noise levels', *Magn. Reson. Imaging*, 2010, **31**, pp. 192–203

[49] Hao, Z., Dong, Z., Hua, Z., *et al.*: 'Applications of nonlocal means algorithm in low-dose X-ray CT image processing and reconstruction: a review', *Med. Phys.*, 2017, **44**, pp. 1168–1185

[50] Nowak, R.D.: 'Wavelet-based Rician noise removal for magnetic resonance imaging', *IEEE Trans. Image Process.*, 1999, **8**, pp. 1408–1419

[51] Wirestam, R., Bibic, A., Lätt, J., *et al.*: 'Denoising of complex MRI data by wavelet-domain filtering: application to high-*b*-value diffusion-weighted imaging', *Magn. Reson. Med.*, 2006, **56**, pp. 1114–1120

[52] Coupé, P., Hellier, P., Prima, S., *et al.*: '3D wavelet subbands mixing for image denoising', *Int. J. Biomed. Imaging*, 2008, p. 11

[53] Martin-Fernandez, F., MuÃ§oz-Moreno, E., Cammoun, L., *et al.*: 'Sequential anisotropic multichannel Wiener filtering with Rician bias correction applied to 3D regularization of DWI data', *Med. Image Anal.*, 2009, **13**, pp. 19–35

[54] Stejskal, E., Tanner, J.: 'Spin diffusion measurements: spin echoes in the presence of time-dependent field gradient', *J. Chem. Phys.*, 1965, **42**, pp. 282–292

[55] Moseley, M.E.: 'Diffusion-weighted MR imaging of anisotropic water diffusion in cat central nervous system', *Radiology*, 1990, **176**, pp. 439–445

[56] Basser, P., Mattiello, J., LeBihan, D.: 'Estimation of the effective self-diffusion tensor from NMR spin echo', *J. Magn. Reson. B*, 1994, **103**, pp. 247–254

[57] Beaulieu, C., Allen, P.S.: 'Determinants of anisotropic water diffusion in nerves', *Magn. Reson. Med.*, 1994, **31**, pp. 394–400

[58] Jones, D.K., Horsfield, M.A., Simmons, A.: 'Optimal strategies for measuring diffusion in anisotropic systems by magnetic resonance imaging', *Magn. Reson. Med.*, 1999, **42**, pp. 515–525

[59] Frank, L.: 'Anisotropy in high angular resolution diffusion-weighted MRI', *Magn. Reson. Med.*, 2001, **45**, pp. 935–939

[60] Frank, L.: 'Characterization of anisotropy in high angular resolution diffusion-weighted MRI', *Magn. Reson. Med.*, 2002, **47**, pp. 1083–1099

[61] Basser, P., Pajevic, S., Pierpaoli, C., *et al.*: 'In vivo fiber tractography using DT-MRI data', *Magn. Reson. Med.*, 2000, **44**, pp. 625–632

[62] Mori, S., Zijl, P.V.: 'Fiber tracking: principles and strategies as a technical review', *NMR Biomed.*, 2002, **15**, pp. 468–480

[63] Parker, G.J.M., Wheeler-Kingshott, C.A.M., Barker, G.J.: 'Estimating distributed anatomical connectivity using fast marching methods and diffusion tensor imaging', *IEEE Trans. Med. Imaging*, 2002, **21**, pp. 505–512

[64] Friman, O., Farneback, G., Westin, C.F.: 'A Bayesian approach for white matter tractography', *IEEE Trans. Med. Imaging*, 2006, **25**, pp. 965–978

[65] Jiang, H., van Zijl, P.C.M., Kim, J., *et al.*: 'DTI studio: a resource program for diffusion tensor computation and fiber bundle tracking', *Comput. Methods Programs Med.*, 2006, **81**, pp. 106–116

[66] Zalesky, A.: 'DT-MRI fiber tracking: a shortest paths approach', *IEEE Trans. Med. Imaging*, 2008, **27**, pp. 1458–1471

[67] Descoteaux, M., Deriche, R., Knosche, T.R., *et al.*: 'Deterministic and probabilistic tractography based on complex fibre orientation distributions', *IEEE Trans. Med. Imaging*, 2009, **28**, pp. 269–286

[68] Pajevic, S., Pierpaoli, C.: 'Color schemes to represent the orientation of anisotropic tissues from diffusion tensor data: application to white matter fiber tract mapping in the human brain', *Magn. Reson. Med.*, 1999, **42**, pp. 526–540

[69] Westin, C.F., Maier, S.E., Mamata, H., *et al.*: 'Processing and visualization for diffusion tensor MRI', *Med. Image Anal.*, 2002, **6**, pp. 93–108

[70] Horsfield, M.A., Jones, D.K.: 'Applications of diffusion-weighed and diffusion tensor MRI to white matter diseases', *NMR Biomed.*, 2002, **15**, pp. 570–577

[71] Masutani, Y., Aoki, S., Abe, O., *et al.*: 'MR diffusion tensor imaging: recent advance and new techniques for diffusion tensor visualization', *Eur. J. Radiol.*, 2003, **46**, pp. 53–66

[72] Dong, Q., Welsh, R.C., Chenevert, T.L., *et al.*: 'Clinical applications of diffusion tensor imaging', *Magn. Reson. Imaging*, 2004, **19**, pp. 6–18

[73] Anderson, W.: 'Measurement of fiber orientation distributions using high angular resolution diffusion imaging', *Magn. Reson. Med.*, 2005, **54**, pp. 1194–1206